Effect of Composition and Austenite Deformation on the Transformation Characteristics of Low-Carbon and Ultralow-Carbon Microalloyed Steels

P. CIZEK, B.P. WYNNE, C.H.J. DAVIES, B.C. MUDDLE, and P.D. HODGSON

Deformation dilatometry has been used to simulate controlled hot rolling followed by controlled cooling of a group of low- and ultralow-carbon microalloyed steels containing additions of boron and/or molybdenum to enhance hardenability. Each alloy was subjected to simulated recrystallization and nonrecrystallization rolling schedules, followed by controlled cooling at rates from 0.1 °C/s to about 100 °C/s, and the corresponding continuous-cooling-transformation (CCT) diagrams were constructed. The resultant microstructures ranged from polygonal ferrite (PF) for combinations of slow cooling rates and low alloying element contents, through to bainitic ferrite accompanied by martensite for fast cooling rates and high concentrations of alloying elements. Combined additions of boron and molybdenum were found to be most effective in increasing steel hardenability, while boron was significantly more effective than molybdenum as a single addition, especially at the ultralow carbon content. Severe plastic deformation of the parent austenite (>0.45) markedly enhanced PF formation in those steels in which this microstructural constituent was formed, indicating a significant effective decrease in their hardenability. In contrast, in those steels in which only nonequilibrium ferrite microstructures were formed, the decreases in hardenability were relatively small, reflecting the lack of sensitivity to strain in the austenite of those microstructural constituents forming in the absence of PF.

I. INTRODUCTION

IN response to the ongoing requirement for steels to exhibit enhanced strength, balanced with high toughness and excellent weldability, new generations of microalloyed steels are being developed.[1] These new steels do not utilize carbon as a major source of enhanced strength, as it is well recognized that high levels of carbon and major alloying elements, apart from increasing strength, may bring about poor weldability and weldment toughness.[1,2] Instead, the alloy design philosophy utilizes very low carbon contents in conjunction with cost-effective microalloying. Suitable combinations of microalloying additions, such as niobium, titanium, molybdenum, or boron, contribute to an increase in strength both directly, through microstructural refinement, solid-solution strengthening, and precipitation hardening, as well as indirectly, through enhanced hardenability and associated modification of the resultant transformation microstructures.[1,3] Optimum product microstructures, with a desired balance of mechanical properties at a given steel composition, are being achieved through suitably designed thermomechanical processing schedules,[4] which commonly involve controlled rolling, followed by controlled accelerated cooling. The controlled rolling step usually includes heavy deformation of the austenite, carried out in the nonrecrystallization-temperature region, which brings about significant refinement of the final transformation microstructures. The accelerated cooling step, designed to take advantage of the increased steel hardenability, aims to suppress the formation of polygonal ferrite (PF) and, instead, encourages nonequilibrium, nonequiaxed ferrite microstructures to be formed. The latter transformation products are known to contribute to increasing strength, through both small effective grain sizes and increased dislocation densities, while maintaining a reasonable level of toughness.[5,6] Although formed in the temperature range typical of classical bainite in medium-carbon steels, the nonequilibrium ferrite microstructures do not contain cementite and possess some unique morphological features.

A specific terminology, proposed recently by the Bainite Research Committee of The Iron and Steel Institute of Japan,[7] has been adopted in the present work in an attempt to describe all possible ferrite morphologies formed by the decomposition of austenite in these modern microalloyed steels with very low carbon contents. Apart from martensite, this terminology recognizes five separate forms of ferrite: (1) PF, the equilibrium microstructural constituent characterized by roughly equiaxed grains with smooth boundaries, mostly containing a low dislocation density and no substructure; (2) Widmanstätten ferrite (WF), defined by elongated crystals of ferrite with a dislocation substructure; (3) quasi-polygonal ferrite (QF), characterized by grains with undulating boundaries which may cross prior-austenite boundaries and containing a dislocation substructure and occasional martensite-austenite (M/A) microconstituents; (4) granular ferrite (GF), which consists of sheaves of elongated ferrite crystals with low misorientations and a high dislocation

P. CIZEK, formerly Research Fellow, Department of Materials Engineering, Monash University, Clayton, Victoria 3168, Australia, is Research Fellow, Department of Materials, University of Oxford, Oxford OX1 3PH, United Kingdom. B.P. WYNNE, formerly Research Fellow, Department of Materials Engineering, Monash University, is Research Fellow, Institute of Microstructural and Mechanical Process Engineering (IMMPETUS), University of Sheffield, Sheffield S1 3JD, United Kingdom. C.H.J. DAVIES, Senior Lecturer, and B.C. MUDDLE, Professor and Head, are with the School of Physics and Materials Engineering, Monash University. Contact e-mail: Chris.Davies@spme.monash.edu.au P.D. HODGSON, Professor and Head, is with the School of Engineering and Technology, Deakin University, Victoria 3217, Australia.

Manuscript submitted May 29, 2001.

density, containing roughly equiaxed islands of M/A microconstituents; and (5) bainitic ferrite (BF), which consists of packets of parallel ferrite laths (or plates) separated by low-angle boundaries and containing very high dislocation densities. In contrast to GF, the M/A microconstituent retained between the ferrite crystals in BF has an acicular morphology.

A quite popular classification system proposed by Bramfitt and Speer[8] has not been adopted in the present investigation, for the reason that it appears to be rather general and does not recognize the specific ferrite morphological types observed in very-low-carbon microalloyed steels. The ferrite morphology denoted BF in the present study has also been termed "acicular ferrite."[9] However, continued use of this term in the present context risks ongoing confusion, as it has been used frequently to describe a range of microstructures observed in microalloyed steels after controlled rolling complemented by accelerated cooling, particularly those dominated by QF.[5] Moreover, the term acicular ferrite is widespread in the welding literature,[10] where it refers to the nonparallel, elongated ferrite crystals formed by particle-induced nucleation in the weld metal. The ferrite morphology denoted QF in the present work has also been referred to as "massive ferrite."[9] The austenite decomposition products containing cementite are generally classified as pearlite (P), degenerate pearlite (P′), and "classical" bainite.[7,9] In order to differentiate between conventional upper bainite (UB) and lower bainite (LB), the classification scheme proposed by Ohmori *et al.*[11] has been adopted.

To obtain greater understanding of the processes that take place during industrial processing of modern microalloyed steels with very low carbon contents, work has recently commenced[12–16] to characterize the transformation behavior and microstructures developed in these steels during laboratory simulations of controlled rolling in conjunction with controlled continuous cooling. This work has indicated that these transformation characteristics might depend significantly on chemical composition as well as processing variables, such as strain in the parent austenite. However, the amount of relevant information available in the literature is, at present, rather limited.[12–16] The aim of the present work was, thus, to undertake a detailed, systematic investigation of the effect of composition and heavy-austenite deformation on the transformation characteristics of a group of low-carbon and ultralow-carbon microalloyed steels containing additions of boron and/or molybdenum to enhance hardenability.

II. EXPERIMENTAL PROCEDURES

The chemical compositions of the steels studied are given in Table I. These steels were vacuum melted as 60 kg ingots and hot rolled to a thickness of 6 mm at BHP Research-Melbourne Laboratories (BHPR-ML). Deformation dilatometry was performed at BHPR-ML using a computerized high-speed quenching and deformation dilatometer. The dilatometry specimens were solid cylinders with a diameter of 4 mm and a length of 8 mm. Each steel was subjected to the simulated recrystallization and nonrecrystallization rolling schedules depicted schematically in Figure 1, followed by controlled cooling at rates from 0.1 °C/s to approximately 100 °C/s. Both rolling schedules included a simulated "roughing" step performed at a temperature of 1100 °C using a strain of 0.30, followed by postdeformation holding at the aforementioned temperature for 120 seconds to ensure complete recrystallization. The simulated nonrecrystallization rolling schedule contained an additional "finishing" step performed at a temperature of 875 °C, which was situated in the nonrecrystallization-temperature region, using a strain of 0.47 in compression. The cooling rates were defined by the time interval required for the specimens to cool from 800 °C to 500 °C. The mean grain diameters of the initial austenite were about 90 and 40 μm for the ultralow-carbon and low-carbon steels, respectively. All specimens were Vickers hardness tested using a 5 kg load and examined by light microscopy after being etched with 2 pct nital. The information obtained was used to construct continuous-cooling-transformation (CCT) diagrams. A more detailed metallographic examination was performed on selected specimens using both scanning electron microscopy and transmission electron microscopy (TEM). Thin foils for TEM were prepared using standard twin-jet electropolishing in an electrolyte consisting of 5 vol pct perchloric acid and 95 vol pct methanol and were examined in a PHILIPS* CM20 transmission electron microscope operating at 200 kV.

*PHILIPS is a trademark of Philips Electronic Instruments Corp., Mahwah, NJ.

III. EXPERIMENTAL RESULTS

A. *Transformation Behavior of Ultralow-Carbon Steels*

1. *Effect of composition*

The CCT diagrams of the ultralow-carbon steels A through D are presented in Figure 2. It is evident that the addition of molybdenum (steel B) to the base composition (steel A) did not cause a significant change in the transformation characteristics (compare Figures 2(c) and 2(a) and also Figures 2(d) and 2(b)). The transformation temperatures for steel B did not differ noticeably from those of steel A. The addition of boron alone (steel C) had a more significant effect on the transformation characteristics of the base steel than the addition of molybdenum. In steel C, the formation of PF was completely suppressed throughout the range of cooling rates studied, even in the case of transformation from the deformed austenite, and all the transformation fields corresponding to the formation of nonequilibrium ferrite constituents were shifted toward the lower-cooling-rate regimes (Figures 2(e) and (f)). As a result, the formation of a mixture of QF and GF extended over the whole range of low to intermediate cooling rates, and the corresponding transformation temperatures became approximately constant throughout this range. Moreover, the transformation field corresponding to the formation of BF was expanded compared to steel A, and some martensite was introduced to the microstructure at the highest cooling rates (compare Figures 2(e) and 2(a) and Figures 2(f) and 2(b)). Nevertheless, no significant differences in the transformation temperatures between steels A and C were detected when comparing transformation products with similar microstructural characteristics.

Combined additions of both boron and molybdenum (steel D) to the base composition did not alter the appearance of the CCT diagrams significantly compared to steel C (compare

Table I. Composition of the Steels Investigated (Weight Percent)

Steel	C	Si	Mn	P	S	Mo	Nb	Ti	B (ppm)
A	0.005	0.189	1.68	0.020	0.010	0.027	0.023	0.014	<1
B	0.007	0.212	1.67	0.021	0.011	0.309	0.024	0.016	<1
C	0.007	0.200	1.64	0.017	0.011	0.008	0.022	0.015	20
D	0.009	0.205	1.70	0.024	0.011	0.273	0.030	0.016	35
E	0.046	0.212	1.64	0.024	0.009	0.045	0.029	0.015	<1
F	0.043	0.210	1.67	0.018	0.011	0.260	0.022	0.016	<1
G	0.043	0.200	1.68	0.019	0.012	0.004	0.021	0.017	20
H	0.044	0.220	1.73	0.019	0.010	0.260	0.022	0.017	19

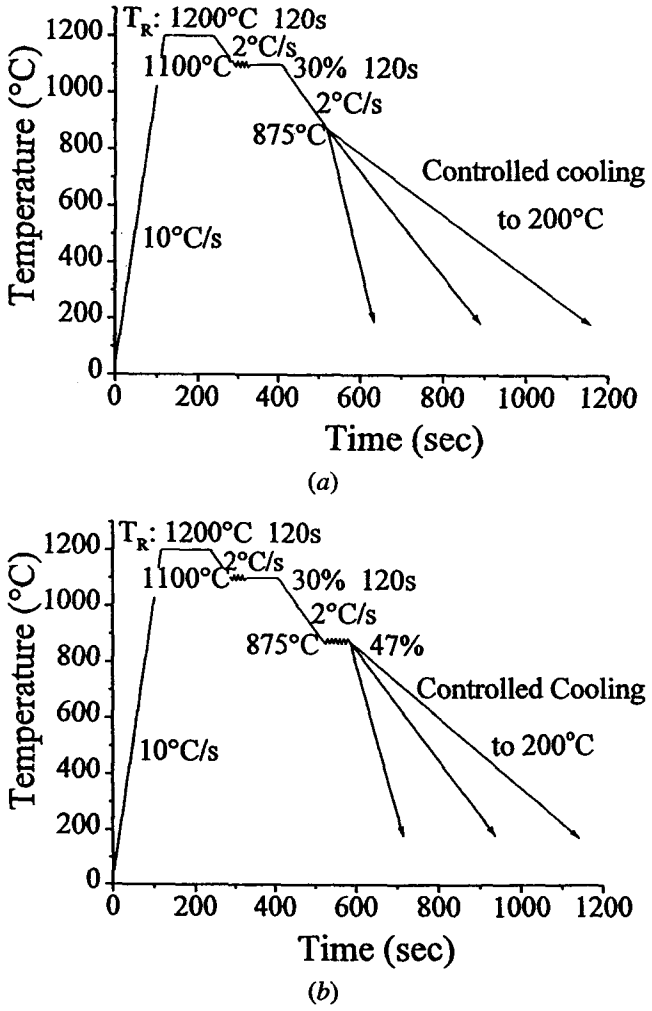

Fig. 1—Schematics of simulated rolling schedules: (*a*) recrystallization schedule and (*b*) nonrecrystallisation schedule involving a strain of 0.47 at 875 °C.

Figures 2(g) and 2(e) and also Figures 2(h) and 2(f)). However, in the case of recrystallized austenite, both the transformation start and transformation finish temperatures in steel D were generally markedly lower than those in steel C (the corresponding maximum temperature decrements were of the order of 55 °C to 60 °C for both the transformation start and finish temperatures). As a result, microstructures mostly composed entirely of GF were formed in steel D in the range of low to intermediate cooling rates, instead of the mixture of QF and GF observed in steel C. In the case of deformed, unrecrystallized austenite, the transformation start temperatures in steel D were similar to those in steel C, whereas the transformation finish temperatures were generally significantly lower (the corresponding temperature decrements ranged from 34 °C to 68 °C).

2. *Effect of austenite deformation*

In steel A, deformation of the prior austenite brought about a significant expansion of the PF transformation field in the CCT diagram (compare Figures 2(b) and 2(a)). The corresponding transformation start temperatures either remained approximately unchanged or underwent only a small increase (the maximum temperature increment was 15 °C). As a guide to this comparison, the open triangles superimposed on Figure 2(b) represent transformation temperatures derived from the corresponding CCT diagrams of the recrystallized austenite (Figure 2(a)) for approximately comparable forms of microstructures. The deviations between these transformation points and those for the deformed austenite (filled circles) are invariably rather small. Such a comparison (also incorporated in Figures 2(d), (f), and (h) and in Figure 3) is necessarily rather crude. Nevertheless, it provides a useful insight into the effect of austenite deformation on the transformation characteristics of a given combination of microstructural constituents, as opposed to simple evaluation of the same effect at equivalent cooling rates, which can be done by a direct overlap of the respective CCT diagrams.

The effect of the parent austenite deformation on the transformation behavior of steel B was found to be similar to that for steel A (compare Figures 2(d) and 2(c)). Steel C appeared to be the least sensitive to austenite deformation of all the steels studied, with the corresponding transformation characteristics remaining basically unchanged (compare Figures 2(f) and 2(e)). Steel D was found to be somewhat more sensitive to the prior-austenite deformation than steel C. As a result of the deformation, the transformation start temperatures for GF formation increased marginally (the corresponding temperature increments ranged from 2 °C to 22 °C), while the transformation finish temperatures remained approximately unchanged. The net transformation range at a given cooling rate was, thus, typically increased (compare Figures 2(h) and 2(g)). Also, deformation of the austenite introduced an increased volume fraction of QF to the GF matrix at the lowest cooling rate (0.1 °C/s). The transformation characteristics of the BF appeared rather insensitive to deformation in steel D.

B. *Transformation Behavior of Low-Carbon Steels*

1. *Effect of composition*

The CCT diagrams for the low-carbon steels E through H are shown in Figure 3. Unlike the case of the ultralow-carbon steel B discussed previously, the individual addition

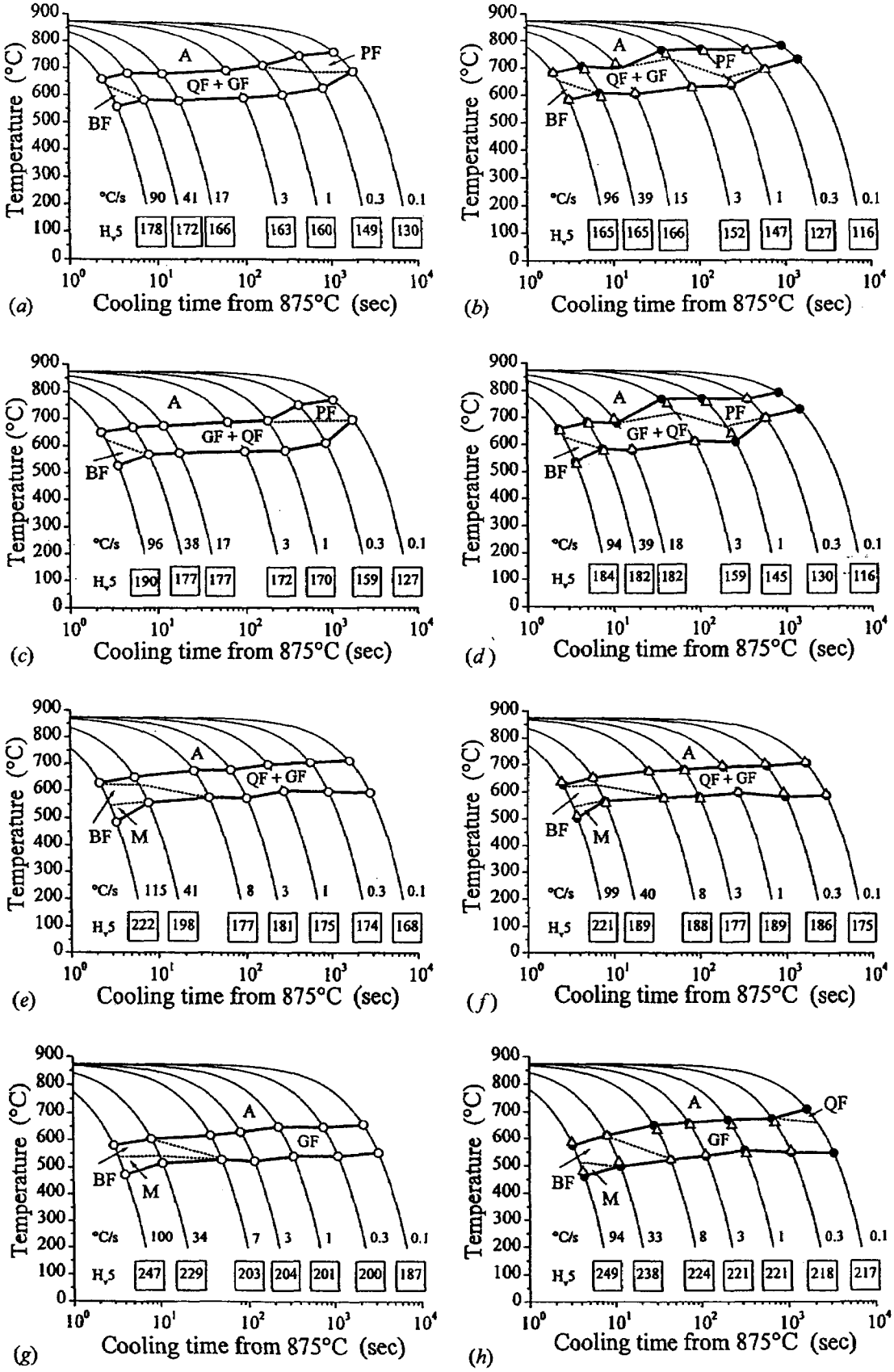

Fig. 2—CCT diagrams for the (*a*), (*c*), (*e*), and (*g*) recrystallized and (*b*), (*d*), (*f*), and (*h*) deformed austenite at the ultralow carbon level: (a and b) steel A, (c and d) steel B, (e and f) steel C, and (g and h) steel D.

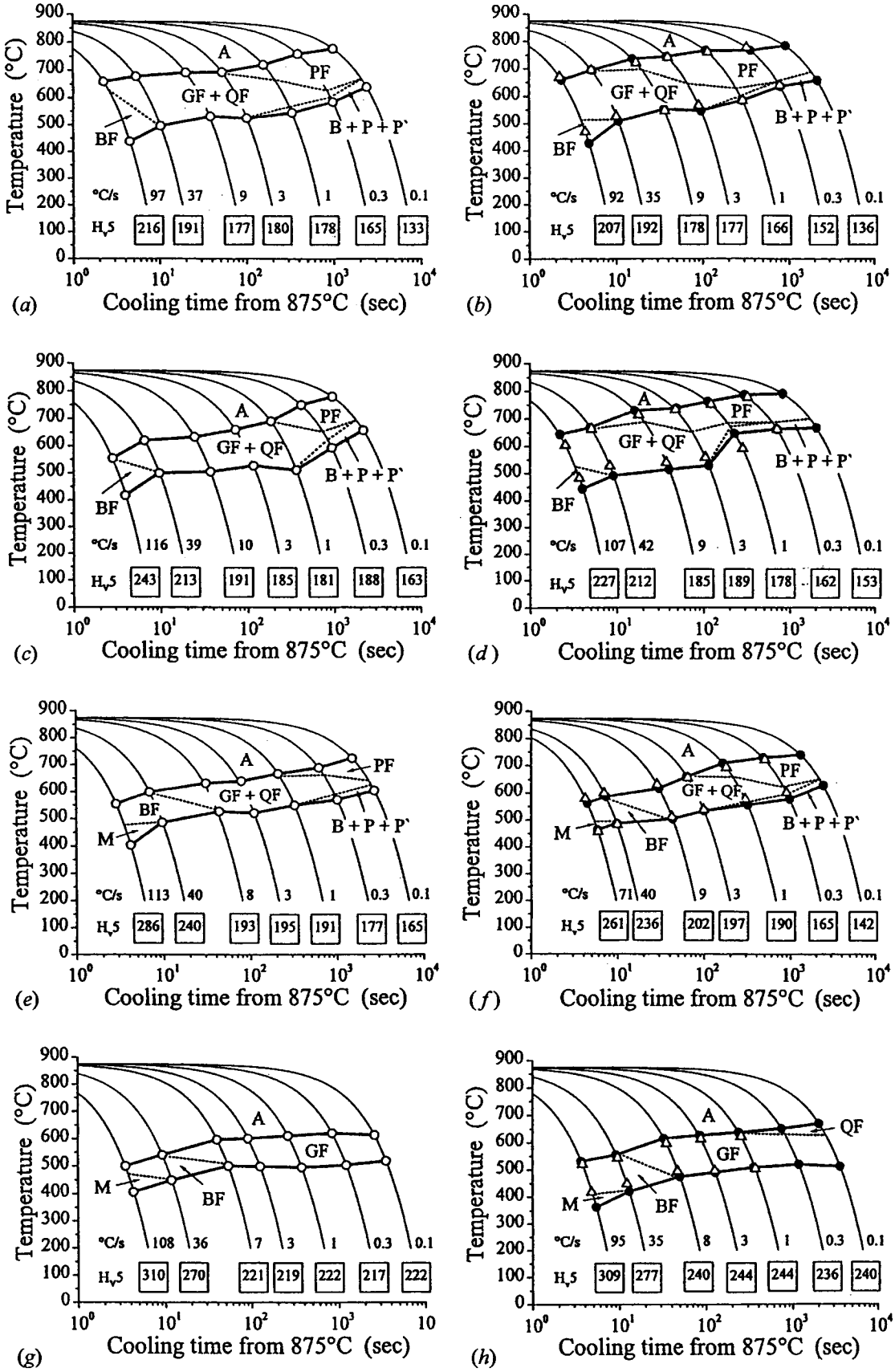

Fig. 3—CCT diagrams for the (*a*), (*c*), (*e*), and (*g*) recrystallized and (*b*), (*d*), (*f*), and (*h*) deformed austenite at the low carbon level: (a and b) steel E, (c and d) steel F, (e and f) steel G, and (g and h) steel H.

of molybdenum (steel F) to the base composition (steel E) brought about somewhat more significant modifications of the CCT diagram for transformation from recrystallized austenite (compare Figures 3(c) and 3(a)). The PF field was slightly reduced and the transformation start temperatures for the formation of the nonequilibrium ferrite constituents decreased noticeably (the corresponding temperature decrements ranged from 31 °C to 105 °C). Nevertheless, the CCT diagrams representing the transformation from deformed, unrecrystallized austenite in steels E and F remained quite similar (compare Figures 3(d) and 3(b)). The addition of boron alone (steel G) brought about significantly enhanced hardenability compared to the base steel E, manifested in a shift of all the transformation fields in the CCT diagram toward the lower-cooling-rate regimes (compare Figures 3(e) and 3(a) and also Figures 3(f) and 3(b)). As a result, the field for PF was reduced in size but, in contrast to the behavior of the boron-containing ultralow-carbon steel C, was not completely eliminated, even in the case of the recrystallized austenite (compare Figures 3(e) and 2(e)). From Figure 3(f), it is evident that the CCT diagram for the deformed austenite of steel G displayed quite a large transformation field for PF. Furthermore, the transformation field for BF was expanded and some martensite was introduced to the microstructure at the highest cooling rates for both the recrystallized and deformed austenite. The temperature intervals at which transformation to the nonequilibrium ferrite constituents occurred were generally reduced significantly in steel G in comparison to steel E, largely as a result of a pronounced decrease in the corresponding transformation start temperatures (the temperature decrements ranged from 27 °C to 60 °C).

The simultaneous additions of boron and molybdenum (steel H) to the base composition had a similar effect to that observed in the ultralow-carbon steel D containing the same microalloying elements. The formation of PF was completely suppressed throughout the entire range of cooling rates studied for the transformation from both recrystallized and deformed austenite (Figures 3(g) and (h)). Compared to steel G containing the addition of boron only, both the transformation start and finish temperatures in steel H were decreased markedly (the corresponding maximum temperature decrements were 58 °C and 53 °C for the transformation start and finish temperatures, respectively), as seen by comparing Figures 3(g) and 3(e) and also Figures 3(h) and 3(f). Consequently, the microstructures observed in this steel at the low to medium cooling rates were mostly composed entirely of GF, rather than of the mixture of QF and GF observed in steel G.

2. *Effect of austenite deformation*

In the low-carbon steels E, F, and G, the austenite deformation caused an expansion of the transformation field for PF in the CCT diagrams (compare Figures 3(b), (d), and (f) with Figures 3(a), (c), and (e), respectively). When comparing transformation products with similar volume fractions of PF, the corresponding transformation start temperatures either remained similar or underwent modest increases (the maximum temperature increments for these steels were less than 20 °C). Thus, the observed response of the transformation behavior of the aforementioned steels to strain in the austenite was quite similar to that found in the ultralow-carbon steels A and B. The expansion of the PF transformation region, observed in steel G, was slightly less significant than that found in either steel E or F, which is consistent with the comparatively smaller PF region present in the CCT diagram of steel G for the recrystallized austenite. The transformation temperatures associated with the formation of the nonequilibrium ferrite microstructures appeared to be mostly rather insensitive to the austenite deformation in this steel. The noticeable deformation-induced decrease in hardenability observed in steel G contrasted sharply with the behavior of its ultralow-carbon counterpart steel C, which did not contain any PF as a result of the decomposition of the deformed austenite (compare Figures 3(f) and 2(f)).

The effects of austenite deformation on the transformation characteristics of steel H were similar to those observed in its ultralow-carbon counterpart steel D at the low to medium cooling rates (compare Figures 3(h) and 2(h)). The transformation-temperature interval for the formation of GF increased slightly, largely as a result of a modest increase in the transformation start temperatures (the corresponding temperature increments ranged from 14 °C to 19 °C). In addition, an increased volume fraction of QF was introduced to the GF matrix at the lowest cooling rates. In contrast, the impact of strain in the austenite on the transformation characteristics of BF, and of mixtures of BF and martensite, was noticeably different from that found in steel D. The corresponding transformation finish temperatures in steel H were reduced significantly (the maximum temperature decrement was 55 °C) and, as a result, the temperature interval of transformation increased.

C. *Transformation Microstructures*

1. *Ultralow-carbon steels*

When the microstructure was composed entirely of PF, which was observed at the lowest cooling rates in steels A and B, the approximately equiaxed ferrite grains did not appear to contain any second-phase islands that would result from decomposition of locally carbon-enriched austenite (Figure 4(a)). This was an expected consequence of the carbon content being well below the solubility limit in ferrite and the cooling rates being sufficiently low to enable diffusion during PF formation to remove any local carbon concentration gradients. Some WF sideplates, extending from polygonal grains, were also observed locally, and their frequency increased with increasing cooling rate. No pronounced dislocation substructure was usually observed within the PF grains.

When PF ceased to be formed, as a result of an increase in cooling rate, the transformation microstructures became dominated by QF, accompanied by some GF. For the microstructures predominantly composed of QF (Figure 4(b)), there was no clear indication of the locations of prior-austenite boundaries. As illustrated in Figure 4(b), QF grains were characterized by irregular boundaries and the presence of clearly etched intragranular subboundaries. Occasionally, some dark-etched fine microregions were also observed within these grains. The aforementioned morphological features made it frequently difficult to distinguish QF grains from often-ragged GF sheaves using light microscopy, especially when large volume fractions of QF were involved. Unambiguous identification of QF areas in mixed regions with GF was often difficult even using TEM, for the reason that these areas often contained dislocation-substructure

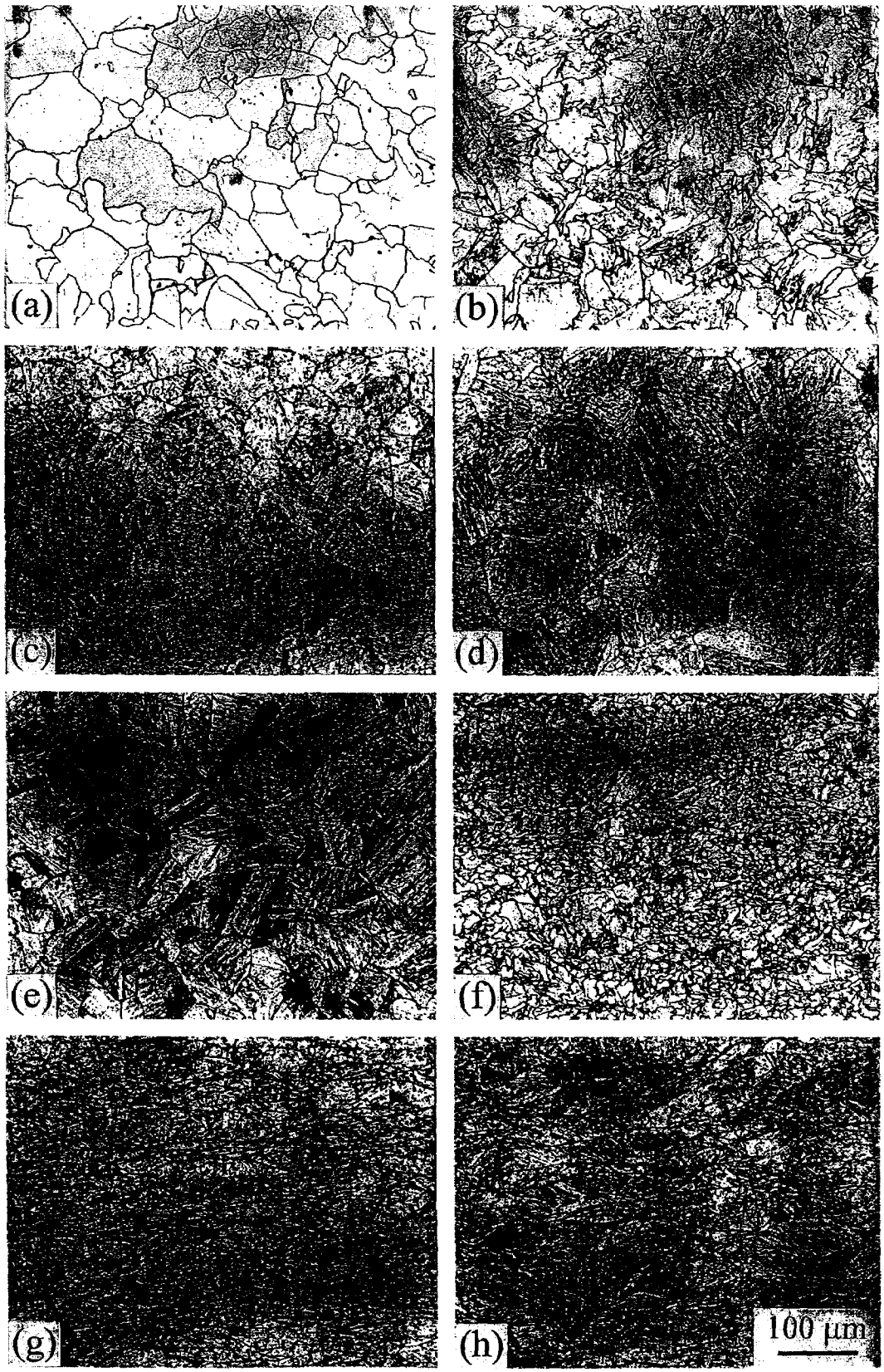

Fig. 4—Light micrographs of the microstructures transformed from the (*a*) through (*e*) recrystallized and (*f*) through (*h*) deformed austenite at the ultralow carbon level: (a) steel A, 0.1 °C/s, PF; (b) steel A, 17 °C/s, QF + GF; (c) steel D, 3 °C/s, GF; (d) steel D, 34 °C/s, BF; (e) steel D, 100 °C/s, BF + M; (f) steel A, 15 °C/s, QF + GF; (g) steel D, 3 °C/s, GF; and (h) steel D, 33 °C/s, BF.

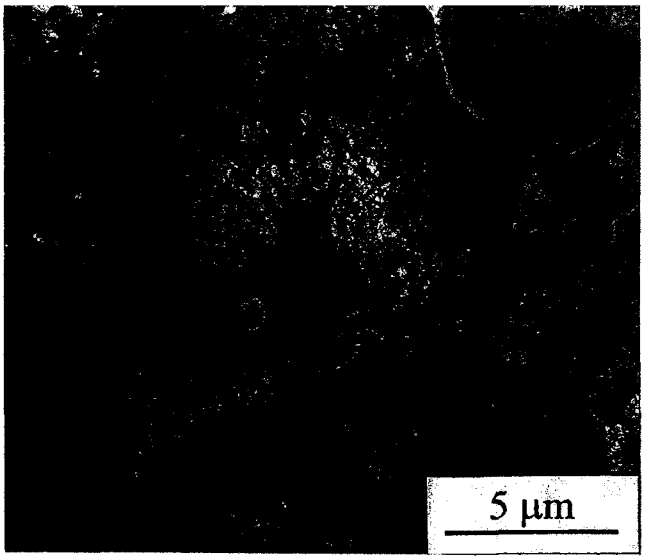

Fig. 5—TEM micrograph of a QF region formed from the recrystallized austenite in steel A at a cooling rate of 17 °C/s.

characteristics similar to GF. Nevertheless, QF did appear to be generally characterized by somewhat coarser substructural fragments and lower dislocation densities in comparison with GF. An example of the dislocation substructure of a region classified as QF is presented in Figure 5. The TEM analysis also revealed that the dark microregions observed by light microscopy contained either bainite or M/A microconstituents the latter being composed of highly dislocated lath martensite.

A gradual increase in cooling rate was accompanied by a continuous rise in the volume fraction of GF at the expense of QF and, at the same time, fine microregions of M/A became more frequent in the light micrographs. When the microstructure contained mostly GF, the locations of prior-austenite grain boundaries were largely preserved (Figure 4(c)). Observed by TEM, the GF sheaves were composed of both elongated and roughly equiaxed fragments, separated by low-angle boundaries and having high internal dislocation densities, and contained approximately equiaxed regions of M/A microconstituents (Figure 6(a)). A further increase in cooling rate brought about a transition from microstructures dominated by GF to those composed predominantly of BF. In light micrographs, the BF was characterized by packets of parallel laths containing very fine, acicular M/A microregions along the lath boundaries (Figure 4(d)). It was generally observed that the higher the cooling rate, the finer the lath width and the scale of the M/A microregions. As illustrated in Figure 4(b), the locations of prior-austenite grain boundaries were entirely retained in this case. In the TEM, the BF laths were separated by low-angle boundaries and contained very high dislocation densities (Figure 6(b)). At the highest cooling rates, some martensite was observed in the microstructures of steels C and D, together with fine BF (Figure 4(e)).

The microstructures, obtained after transformation from the deformed, unrecrystallized austenite, differed noticeably from those formed from recrystallized austenite. Both PF and QF grains were significantly refined (compare Figures 4(f) and 4(b)), and a similar trend was observed for both GF sheaves and BF packets (compare Figures 4(g) and 4(c) and also Figures 4(h) and 4(d)). The GF substructures were found to be slightly more fragmented, but there was no obvious increase in the corresponding dislocation densities as a result of transformation from heavily deformed austenite (compare Figures 6(c) and 6(a)). The BF laths generally became shorter (compare Figures 6(d) and 6(b)), along with the decrease in the corresponding packet dimensions.

2. *Low-carbon steels*

In general, comparatively finer-scale microstructures were observed by light microscopy in steels E through H compared to steels A through D, as a result of transformation from finer-scale austenite. The microstructures of the low-carbon steels were found to be somewhat more complex than those of the ultralow-carbon steels in the range of low to medium cooling rates leading to the formation of PF. Although the morphology of PF grains observed in steels E through G was generally similar to that found in steels A and B (compare Figures 7(a) and (b) and Figure 4(a)), some of the former grains contained clear traces of subboundaries. Volume fractions of the PF grains with a pronounced dislocation substructure were particularly high in steel G, and these grains frequently contained WF sideplates. The TEM analysis revealed that such grains were characterized by an increased density of dislocations arranged in both complex tangles and planar low-angle walls (Figure 8). Moreover, due to the carbon content exceeding the solubility limit in ferrite, the microstructure of PF grains in steels E through G contained carbon-enriched islands comprising a complex mixture of austenite decomposition products. At the lowest cooling rates, the carbon-enriched regions displayed quite uniform dark-etching contrast in light micrographs (Figure 7(a)), and TEM showed that they were predominantly composed of bainite, accompanied by a small amount of fine P or P′ (Figure 9(a)). The observed bainite morphology could be best classified as a mixture of BII and BIII upper bainite, according to the scheme proposed by Ohmori *et al.*[11]

The BII sheaves were composed of highly dislocated ferrite laths separated by continuous cementite layers, while the BIII sheaves, which were observed much more frequently than BII, contained discrete cementite platelets aligned along a common direction within the ferrite matrix (Figures 9(a) and (b)). Occasionally, a small volume fraction of LB was also observed locally within the carbon-enriched islands (Figure 9(c)). In this case, cementite was present in the form of fine platelets inclined toward the long axes of the LB sheaves. As also illustrated in Figure 9(c), cementite-free "spines" were found within these sheaves, and it has been suggested by Spanos *et al.*[17] that these might represent the regions where LB formation was initiated. With increasing cooling rates, the PF volume fraction gradually decreased and the rest of the microstructure became characterized by dark-etching microregions scattered within white ferritic areas (Figure 7(b)). In the TEM, the microregions displaying the dark-etching response in light micrographs were composed predominantly of bainite, with only a small fraction of fine P′. The ferrite matrix, in which the dark-etching particles were embedded, contained a high dislocation density and was subdivided into fragments separated by low-angle boundaries. Thus, such a microstructure appeared to be similar to that observed within the GF sheaves formed at higher-cooling-rate regimes (as noted subsequently), apart

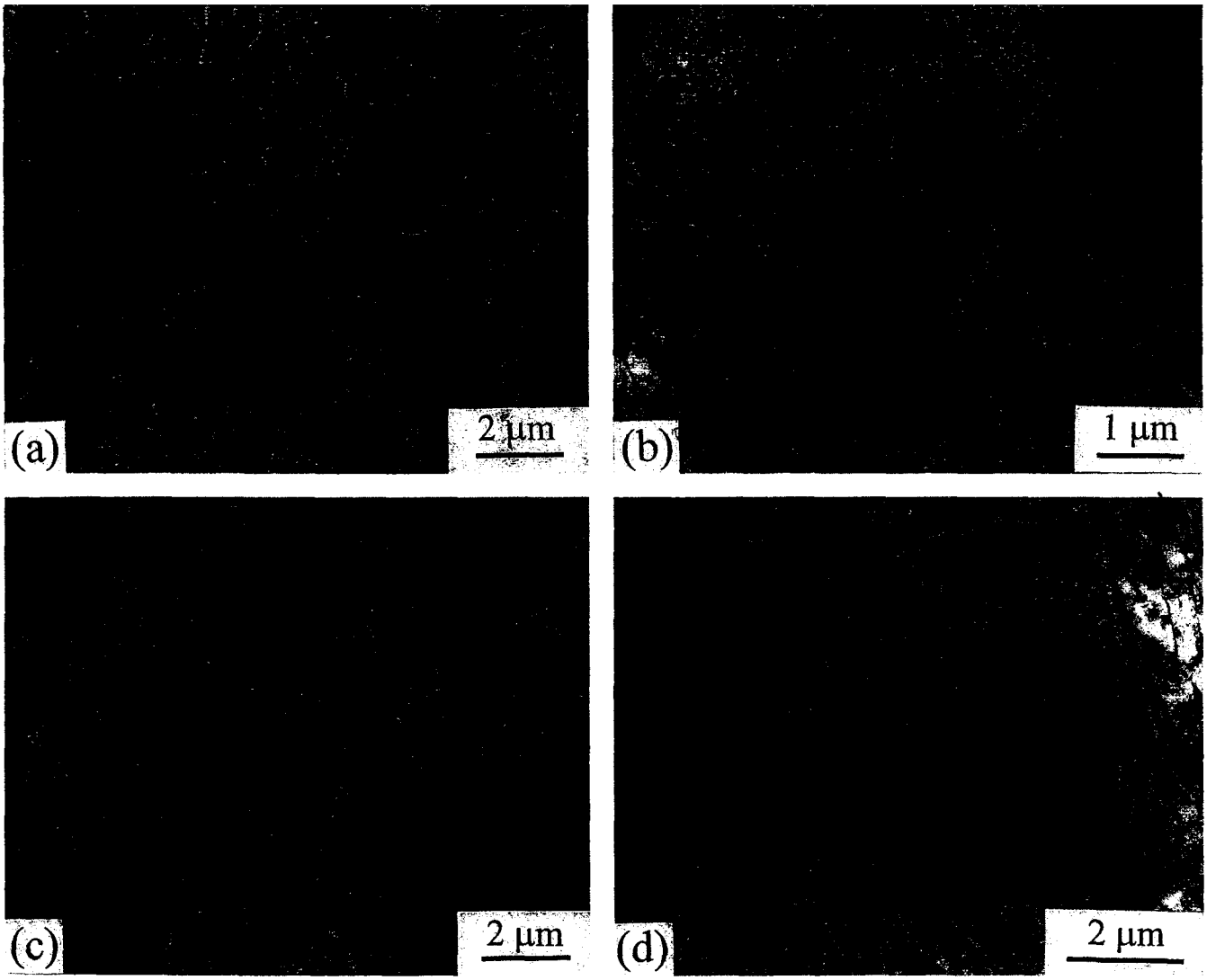

Fig. 6—TEM micrographs of the nonequilibrium ferrite microstructures, containing M/A microconstituents, transformed from the (*a*) and (*b*) recrystallized and (*c*) and (*d*) deformed austenite in steel D: (a) 3 °C/s, GF; (b) 34 °C/s, BF; (c) 3 °C/s, GF; and (d) 33 °C/s, BF.

from the second-phase microregions being coarser and composed largely of bainite rather than M/A microconstituents typical of GF.

When the cooling rate increased above a certain limiting level, PF ceased to be formed and the transformation microstructure became dominated by QF (Figure 7(c)), accompanied by GF. The QF grains displayed similar morphological and substructural characteristics to those observed in the ultralow-carbon steels (compare Figures 7(c) and 4(b)). However, as expected, in steels E through H, these grains contained significantly larger volume fractions of comparatively coarser distributed microconstituents, composed of a mixture of dark-etching bainite microregions and grey-contrast M/A microconstituents. A gradual increase in cooling rate was accompanied by a parallel increase in the volume fraction of GF in the microstructure, at the expense of QF, and the distributed microregions became dominated by M/A microconstituents. The latter comprised a number of variants of highly dislocated lath martensite, accompanied by barely detectable retained austenite. They occasionally contained microtwins within the martensite, suggesting a significant local enrichment in carbon (Figure 10). Both the morphology and substructure of the GF sheaves resembled those observed in steels A through D (compare Figures 7(d) and 4(c) and also Figures 11(a) and 6(a)), but there was a larger fraction of coarser M/A microconstituents detected in the low-carbon steels E through H. A further increase in cooling rate brought about a transition from GF to BF and, ultimately, the formation of a significant volume fraction of martensite. The presence of coarser and more numerous acicular M/A microregions in the low-carbon steels was again the major difference between the BF microstructures of comparable steels at the two carbon levels (compare Figures 7(e) and 4(d) and also Figures 11(b) and 6(b)). The differences in microstructural characteristics between the transformation products formed from the heavily deformed austenite and from the recrystallized austenite were similar for steels E through H to those described previously for the ultralow-carbon steels (compare the light micrographs in Figures 7(g) and 7(d) and also in Figures 7(h) and 7(f), or the TEM micrographs in Figures 11(c) and 11(a) and also in Figures 11(d) and 11(b)).

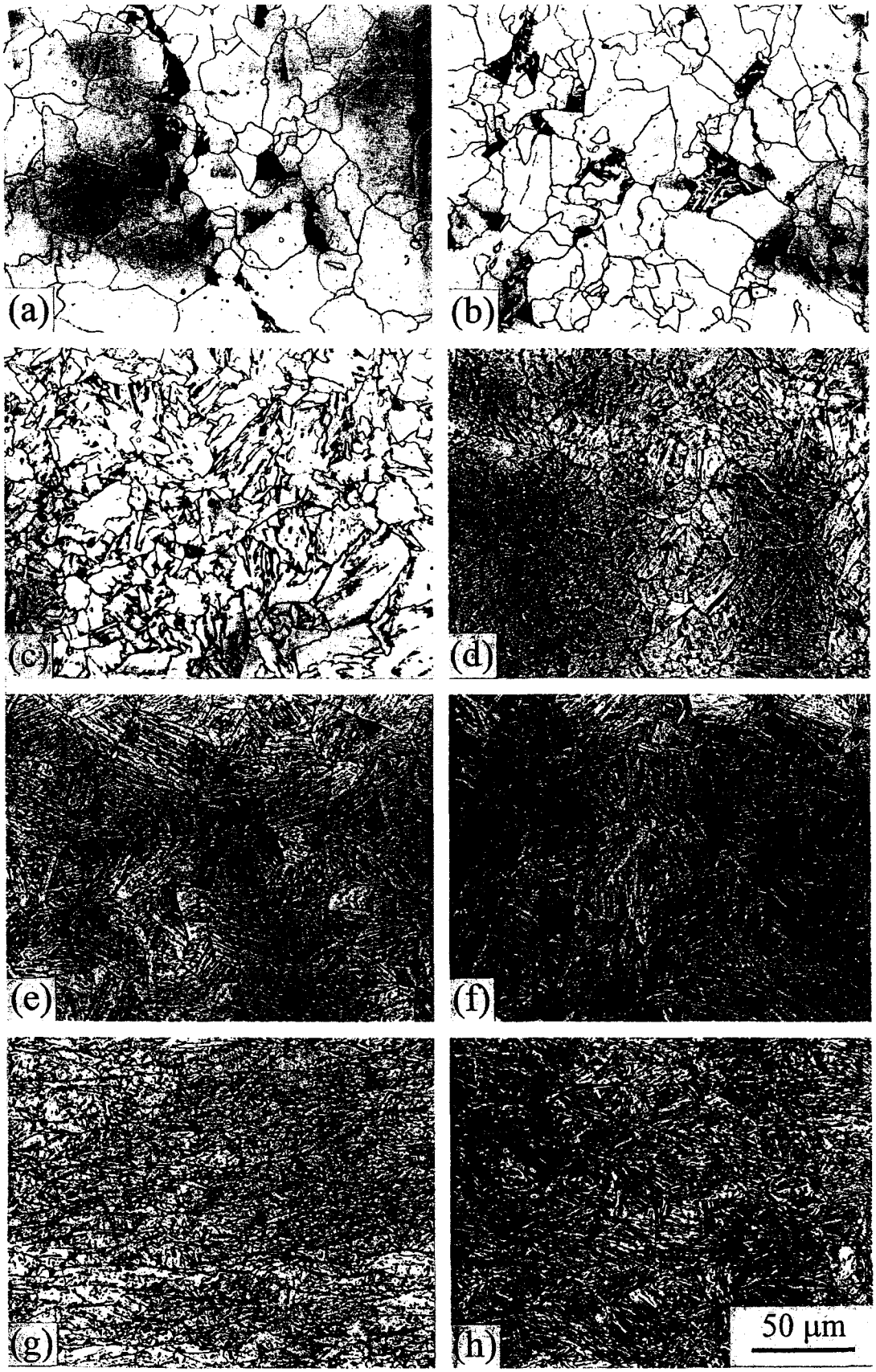

Fig. 7—Light micrographs of the microstructures transformed from the (*a*) through (*f*) recrystallized and (*g*) and (*h*) deformed austenite at the low carbon level: (a) steel E, 0.1 °C/s, PF; (b) steel E, 0.3 °C/s, PF + GF; (c) steel E, 3 °C/s, QF + GF; (d) steel H, 3 °C/s, GF; (e) steel H, 36 °C/s, BF; (f) steel H, 108 °C/s, M + BF; (g) steel H, 3 °C/s, GF; and (h) steel H, 95 °C/s, BF + M.

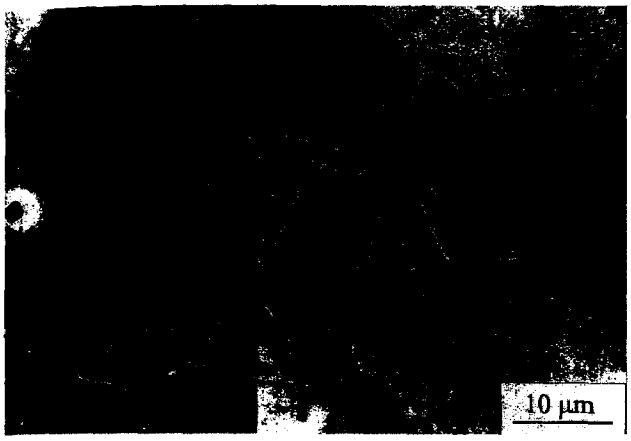

Fig. 8—TEM micrograph of a PF grain with a pronounced dislocation substructure formed from the recrystallized austenite in steel G at a cooling rate of 0.3 °C/s.

D. *Hardness Measurements*

Measurements of the bulk Vickers hardness of each of the dilatometer specimens are superimposed on the CCT diagrams in Figures 2 and 3. Each value reported is the average of five individual measurements performed in the central area of a longitudinal section of a given sample. These data are summarized in Figure 12, where hardness values are plotted separately for each carbon level studied as a function of either cooling rate (Figures 12(a) and (c)) or austenite-ferrite transformation start temperature (Figures 12(b) and (d)). The hardness values of the ultralow-carbon steels A through D were found to be systematically lower than those of their low-carbon counterparts E through H at the same content of microalloying elements. It is clear from Figures 12(b) and (d) that for both carbon levels, the hardness data conform to an approximately linear relationship as a function of transformation temperature, with the hardness increasing systematically with decreasing austenite-ferrite transformation start temperatures. For the matrix of steels examined, there was no significant influence of steel composition on the form of this relationship detected in the present measurements. As expected, the lowest hardness values observed correspond to the microstructures dominated by PF, which formed at the highest transformation start temperatures. Conversely, the highest hardness values were displayed by the microstructures composed of BF and martensite, forming at the lowest transformation start temperatures. The hardness data obtained for QF and GF, characterized by intermediate formation temperatures, were situated between the aforementioned limits. As illustrated in Figures 12(a) and (c), in steels C, D, and H, microstructures dominated by GF displayed pronounced hardness plateaus extending over a wide range of cooling rates.

The transformation microstructures formed from the deformed parent austenite were generally observed to display increased hardness values compared to the equivalent microstructures created from the recrystallized austenitic matrix (Figures 2 and 3). These hardness increments are generally not obvious from Figures 12(a) and (c), where the comparison between hardness values is made at similar cooling rates rather than for similar microstructures. They are better illustrated in Figures 12(b) and (d), where comparable microstructures are roughly approximated by similar transformation start temperatures, and hardness values for samples produced from deformed austenite (filled symbols) are systematically higher than those from recrystallized austenite (open symbols).

IV. DISCUSSION

A. *Transformation Behavior*

1. *Effects of composition*

An increase in the hardenability of the austenite generally manifested itself, during its decomposition, by suppressing the formation of PF and of QF and promoting the formation of GF, BF, and martensite. The addition of molybdenum alone (steels B and F) slightly increased the hardenability of the base steel at the low-carbon level, while there was barely a detectable change in hardenability observed at the ultralow-carbon content. The individual addition of boron to the base steel composition was significantly more effective in promoting hardenability than that of molybdenum, markedly restricting the formation of PF in the low-carbon steel G and completely eliminating its formation in the ultralow-carbon steel C for the entire range of cooling rates studied. An especially large increase in hardenability was achieved by the combined additions of molybdenum and boron to the base steel, which is consistent with published data,[18] and there was no noticeable difference in the resultant hardenability of steels for the two carbon levels studied (steels D and H). The transformation temperatures were lowered significantly, the formation of PF was entirely eliminated, and that of QF was markedly suppressed.

The factors that control austenite hardenability in microalloyed steels appear to be rather complex and not fully understood at the present time. It has been generally accepted that alloying elements tend to increase austenite hardenability.[1,19] Austenite stabilizers, such as manganese, carbon, and nitrogen, retard the austenite decomposition by lowering the Ar_3 temperature, thus reducing the overall undercooling (the transformation driving force) at a given transformation temperature. Ferrite stabilizers, such as silicon, molybdenum, niobium, and titanium, although raising the Ar_3 temperature, similarly retard the decomposition of austenite, largely *via* reducing the diffusivity of carbon in this constituent.[1,19] It has been suggested[1,16,18,20,21] that niobium, titanium, molybdenum, and boron in particular, tend to segregate to the prior-austenite grain (and deformation-induced) boundaries. These alloying elements may possibly reduce the ferrite nucleation rate *via* the formation of either extremely fine carbonitride/carboboride precipitates or preprecipitation clusters with carbon, which cover the aforementioned boundaries and, thus, hinder the ferrite nucleation.[18,22,23] An estimated reduction in the austenite grain-boundary energy, resulting from the presence of the aforementioned elements as segregated atoms, does not appear to be large enough to correlate with the observed decrease in the corresponding ferrite nucleation rate.[22–24] Thus, the aforementioned alloying elements could be expected to decrease the nucleation rates of all the ferrite morphological types nucleating heterogeneously on the austenite grain or deformation-induced boundaries.

It has been reported[1,16,25,26] that substitutional alloying

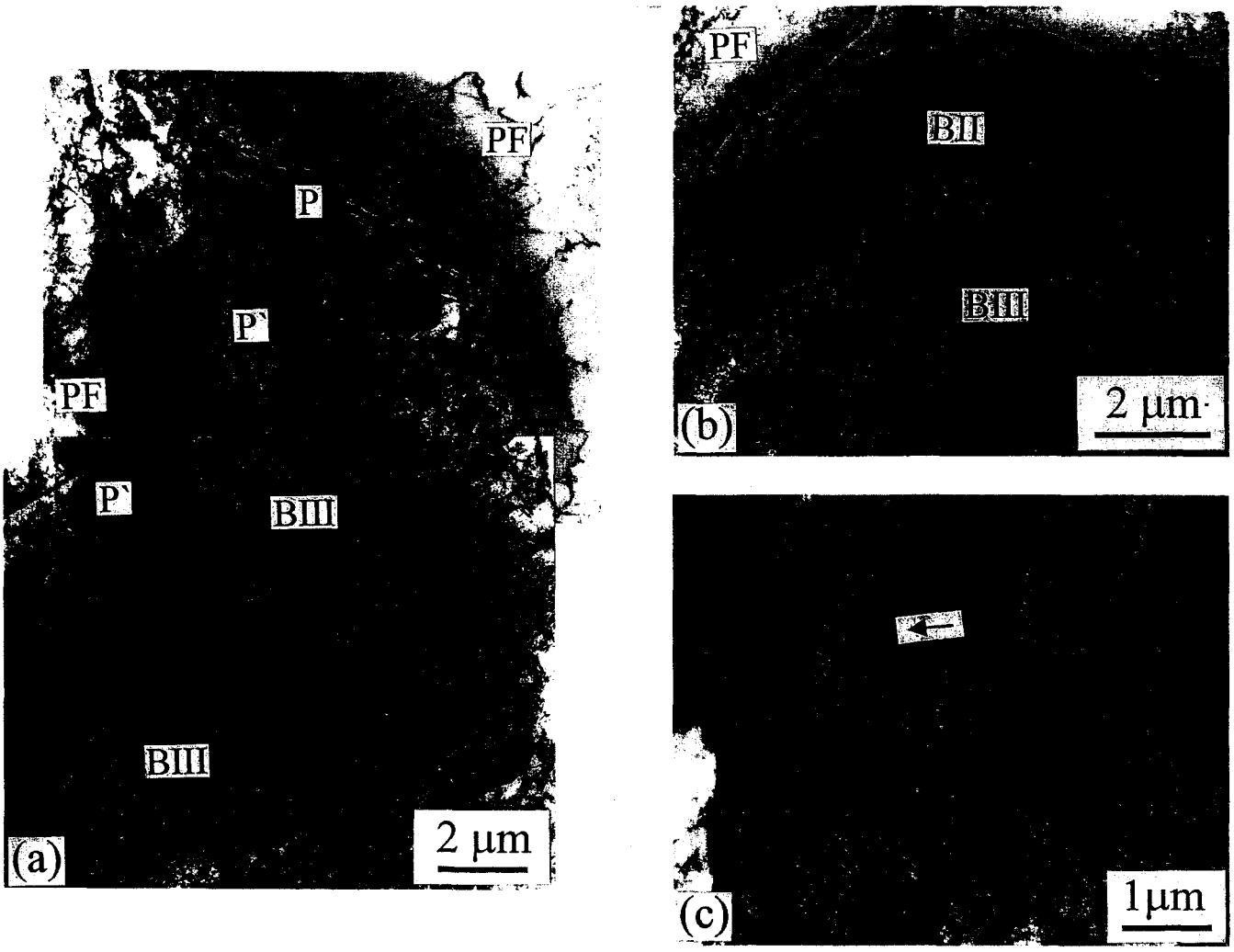

Fig. 9—Substructure of the carbon-enriched regions present within the PF matrix in steel E after transformation from the recrystallized austenite at a cooling rate of 0.1 °C/s: (*a*) BIII + P + P′, (*b*) BIII + BII, and (*c*) LB. Arrow in (c) indicates a cementite-free "spine."

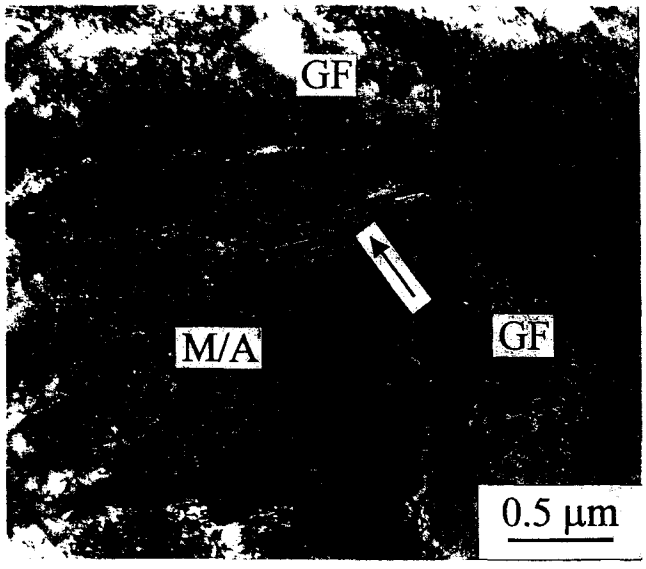

Fig. 10—TEM micrograph of a M/A microregion, composed of both lath and twinned martensite (arrowed), observed within GF formed from the recrystallized austenite in steel H at a cooling rate of 3 °C/s.

elements such as manganese, molybdenum, niobium, or titanium tend to reduce the ferrite growth rate. There have been suggestions[25,26] that this phenomenon might be a consequence of a solute drag–like effect (SDLE). According to the SDLE hypothesis,[25] nonequilibrium adsorption of the aforementioned elements, having appreciable size misfits with respect to the iron atoms, occurs to the disordered areas close to the ferrite/austenite interface during ferrite growth. Since these solute elements suppress the carbon activity in the austenite in contact with the growing ferrite, they reduce the diffusional flux of carbon into austenite and, thus, the resulting ferrite growth rate. It is necessary to note, however, that applicability of the SDLE concept to the case of the nonequilibrium ferrite constituents is based on the premise that these are formed *via* a diffusion-controlled ledge growth,[27] which is still a matter of dispute.[28,29,30]

The observed rather weak contribution of molybdenum (at the level of about 0.3 wt pct) to the hardenability enhancement of the base steels, compared to boron, might partly originate from the presence of the simulated roughing step in the processing schedules used in the present study (Figure 1). It appears reasonable to suggest that static recrystallization occurring during the isothermal holding at 1100 °C

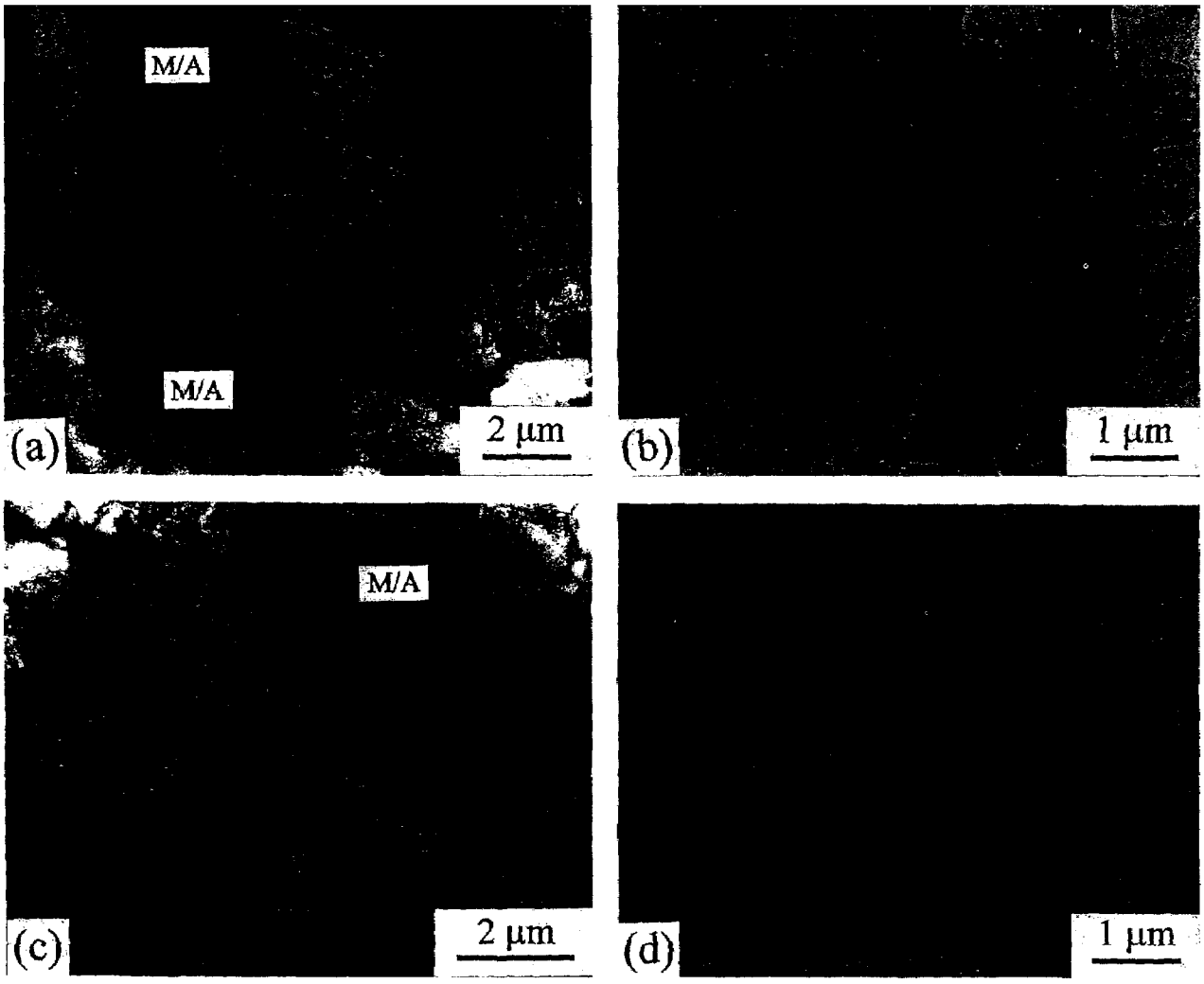

Fig. 11—TEM micrographs of the nonequilibrium ferrite microstructures, containing M/A microconstituents, transformed from the (*a*) and (*b*) recrystallized and (*c*) and (*d*) deformed austenite in steel H: (a) 3 °C/s, GF; (b) 36 °C/s, BF; (c) 3 °C/s, GF; and (d) 35 °C/s, BF.

(following the application of a roughing strain of 0.30) and accompanied by the movement of the austenite grain boundaries might have prevented molybdenum from segregating effectively to these boundaries. Consequently, the addition of molybdenum could be expected to have only a limited effect on the nucleation rate of ferrite under the present experimental conditions. The hardenability enhancement probably originated mainly from the effect of molybdenum in solid solution and, thus, was largely restricted to the lowering of the ferrite growth rate, perhaps *via* a SDLE.[25,26]

Boron, on the other hand, as an interstitial element characterized by high diffusivity in austenite, could be expected to segregate relatively readily to both the recrystallized austenite grain boundaries formed during the simulated roughing step and the deformation-induced boundaries created during the simulated finishing step performed at 875 °C. Thus, as generally accepted,[16,18,20] boron appeared to enhance the hardenability primarily through suppressing the ferrite nucleation rate. The significant increase in hardenability of the base steels due to the boron addition, as observed in the present study, appears likely to be largely a consequence of the combined additions of boron and niobium. These two elements have been reported to act synergistically to enhance hardenability significantly more than might be expected from an individual addition of boron in the absence of niobium.[16,18] In order to account for this phenomenon, it has been suggested[16,18] that the addition of niobium, which is a stronger carbide or nitride former than boron, tends to encourage precipitation of niobium carbonitrides, which limits the supply of carbon for the precipitation of carboborides. Consequently, boron is maintained in solid solution, and its potential for segregation to all possible ferrite nucleation sites is, thus, increased. This effect might be expected to intensify with a decreasing carbon content,[16,18] which is consistent with the particularly significant increase in hardenability observed in the ultralow-carbon steel C.

From the previous findings, it is clear that the particularly large increase in hardenability, achieved by the combined additions of molybdenum and boron to the base steels, cannot

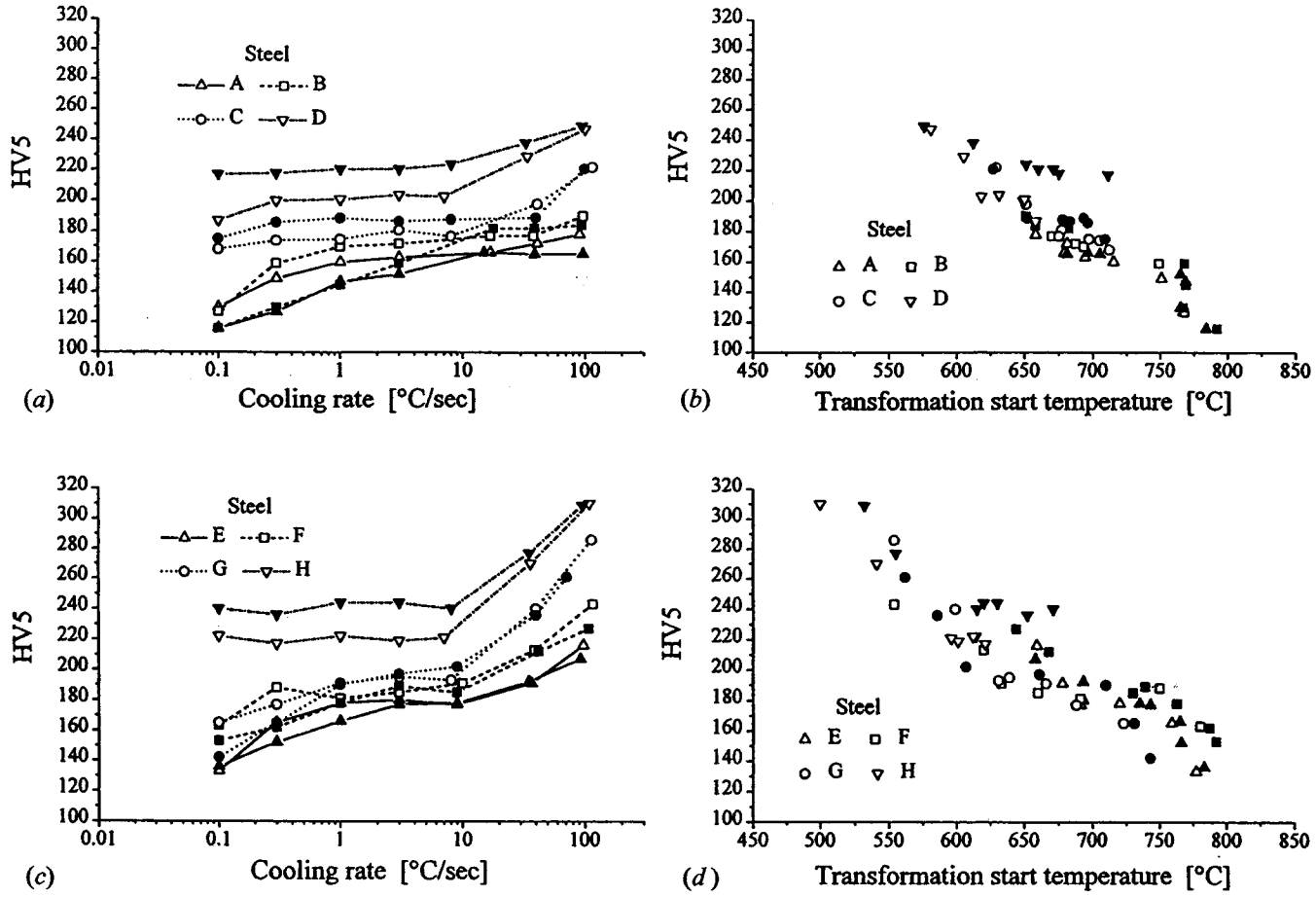

Fig. 12—Hardness characteristics plotted as a function of either (*a*) and (*c*) cooling rate or (*b*) and (*d*) transformation start temperature: (a and b) ultralow-carbon steels and (c and d) low-carbon steels. Open and filled symbols correspond to the transformation products formed from the recrystallized and unrecrystallized austenite, respectively.

be explained as a simple superposition of the individual effects of these two elements. The observed hardenability increase clearly resulted from an especially strong synergistic effect of molybdenum and boron at the presence of niobium, which is agreement with published data.[18] Nevertheless, the exact nature of this effect still remains to be clarified.

2. *Effects of austenite deformation*

Heavy deformation of austenite, carried out at a temperature (875 °C) situated below the nonrecrystallization limit, quite markedly enhanced formation of PF in the ultralow-carbon steels A and B, as well as in the low-carbon steels E through G, significantly extending its presence in the CCT diagrams to the higher cooling rates. The observation of a pronounced shift of the PF transformation fields toward higher cooling rates as a result of prior-austenite deformation is consistent with published data.[12,15] It has sometimes been claimed that this shift is also accompanied by a significant increase in the corresponding transformation start temperatures.[15] However, this phenomenon appears to be mainly a consequence of comparing these temperatures at a similar cooling rate rather than for a similar microstructure, as has been done in the present study. The present results indicate modest increases in the transformation temperatures for PF as a result of prior-austenite deformation; the corresponding temperature increments were always less than 20 °C.

It has been widely accepted[15,31,32] that the enhanced PF formation, and a concomitant decrease in hardenability, brought about by the heavy deformation of austenite may be largely attributed to an increase in the ferrite nucleation rate, while the ferrite growth rate seems to be less affected. This suggestion appears to be supported by the significantly finer PF grain size obtained in the present study after transformation from the deformed austenite, compared to the case of the recrystallized austenite. As a result of the austenite deformation, a density of ferrite nucleation sites is expected to increase. The reason for this is that straining leads to both an increase in the austenite grain-boundary area per unit volume as a consequence of the grain flattening[31] and to the formation of deformation bands or shear bands known to serve as potent ferrite nucleation sites.[31,33,34] Moreover, deformation of austenite also appears to convert the originally low-energy coherent interfaces of annealing twins into high-energy incoherent interfaces suitable for ferrite nucleation.[35] Apart from increasing the density of ferrite nucleation sites, austenite deformation creates a high density of dislocations, the strain energy of which raises the austenite free energy, which, in turn, brings about a certain reduction

in the critical free energy for ferrite nucleation.[31] Also, the heavy austenite deformation, performed at 875 °C in the present study, could be expected to decrease the amount of niobium in solid solution due to strain-induced precipitation of niobium carbonitrides.[12,15,31] This would tend to increase both the ferrite nucleation and growth rates due to the lowering of the amount of niobium available for segregation or SDLE, respectively. The ferrite growth might be also somewhat accelerated due to enhanced pipe diffusion along the dislocations in the austenite but, conversely, it could be locally suppressed by pinning of the advancing ferrite/austenite interfaces by the fine strain-induced niobium carbonitrides.

The austenite deformation also appeared to promote QF formation, as clearly evidenced by the observed slightly enhanced formation of this constituent in steels D and H at the lowest cooling rates. This is consistent with previous observations[14] and might be explained by an increase in the ferrite nucleation rate, in analogy to the case of PF discussed previously. It appears reasonable to suggest that, although QF nucleation could be expected to be enhanced in steels D and H throughout a wide range of cooling rates, the QF grains formed at the lowest cooling rates became more noticeable in the microstructure, compared to those formed at higher cooling rates, thanks to the significantly longer time periods available for their growth. The effect of the austenite deformation on the transformation temperatures for QF proved difficult to estimate, as this microstructural constituent was mostly present in complex mixtures with GF, but any changes in the transformation start temperatures did not seem to be particularly significant.

In steels D and H, GF was formed almost entirely without QF, which allowed the effect of the austenite deformation on its transformation characteristics to be evaluated. It appears that GF nucleation was slightly accelerated and the progress of the transformation was generally slightly retarded, while the corresponding transformation field did not appear to expand toward the higher cooling rates. Although the observed accelerated nucleation of GF might be explained using the same arguments as those used previously, an interpretation of the retarded growth would require the knowledge of the GF formation mechanism, which has not yet been firmly established. The pinning of the ferrite/austenite interfaces by fine strain-induced carbonitrides, or perhaps the mechanical stabilization phenomenon,[36] might be put forward as possible explanation candidates. The effect of the austenite deformation on the transformation characteristics of BF proved difficult to estimate due to both the narrow range of cooling rates at which this constituent was formed and the interference of martensite formation. Nevertheless, these characteristics appeared, for the most part, rather insensitive to deformation of the parent austenite in the steels investigated.

From the aforementioned findings, it is clear that, as a result of the heavy austenite deformation, the formation of PF in the present study was enhanced noticeably more than that of the nonequilibrium ferrite constituents, which is in agreement with the findings presented by Tamehiro *et al.*[16] This indicates that the transformation mechanisms of the latter constituents might be significantly less sensitive to deformation than that of PF. Thus, it may be concluded that enhanced PF formation was primarily responsible for the decrease in hardenability resulting from the austenite deformation in the steels studied.

B. *Transformation Microstructures*

The PF grains observed in the ultralow-carbon steels A and B were characterized by relatively high transformation temperatures (Figures 2(a) through (d)) and mostly contained low densities of dislocations. In the low-carbon steels E through G, PF grains were formed over a comparatively wider range of transformation temperatures (Figures 3(a) and (f)), as the corresponding transformation finish temperatures were mostly significantly lower than those for steels A and B. Some of the latter grains contained increased densities of dislocations, arranged in both complex tangles and planar low-angle walls. Volume fractions of such PF grains having a pronounced dislocation substructure were particularly significant in steel G, characterized by rather low PF transformation temperatures (the maximum corresponding transformation start temperatures were 723 °C and 743 °C for the recrystallized and deformed austenite, respectively). These observations might be interpreted using the concept suggested by Wilson.[37,38] According to this concept, PF formation at comparatively high transformation temperatures is characterized by a relatively small degree of undercooling below the metastable equilibrium temperature T_0. Thus, the resultant small driving force for the transformation might be aided by PF nucleation at austenite grain corners with one or more (semi-)coherent interfaces, which would reduce the activation-energy barrier to nucleation. Consequently, the volume change accompanying PF formation could be fairly easily absorbed by the grain boundaries at the high transformation temperatures involved, which is in agreement with the low dislocation densities observed inside PF grains formed at these temperatures. Conversely, PF formation at comparatively lower transformation temperatures is characterized by a somewhat larger relative undercooling below T_0. Thus, as a result of the relatively larger chemical driving force for the transformation, PF grains might nucleate as hemispherical caps on the austenite grain faces with only one planar (semi-)coherent interface. In this case, due to both the shape of the nuclei and the lower transformation temperatures, the volume change accompanying PF formation cannot be expected to be completely absorbed by the grain boundaries. This would result in the introduction of the observed increased densities of accommodation dislocations to the interiors of the PF grains formed at comparatively lower transformation temperatures. As expected from the theory of deformation-microstructure evolution,[39] these dislocations were arranged in complex tangles and, locally, in planar "dense dislocation walls."

When the carbon content exceeds the solubility limit in PF, carbon-enriched austenite regions, stabilized against further PF formation, may form during the transformation, as was observed in steels E through G. The carbon-enriched austenite was found to subsequently undergo complex decomposition during further cooling, presumably due to variations in carbon enrichment. Small fractions of P or P′, observed within the carbon-enriched islands at the very low cooling rates, suggest that the pearlite transformation field was occasionally intersected in some local volumes during

cooling. The bulk of the carbon-rich austenite transformed into UB accompanied by only small fractions of LB. Thompson *et al.*[40] have suggested that, in addition to carbon enrichment, significant undercooling might also be required for bainite to nucleate in the carbon-enriched regions. This would require a low-temperature bainite transformation field in the CCT diagram in the region of low cooling rates, perhaps separated from that of PF by a metastable austenite region.[40] However, such a transformation field could not be located for steels E through G, presumably due to the lack of sensitivity of dilatometry utilizing solid specimens.

Unlike the PF grains described previously, their QF counterparts were observed to display ragged boundaries and a pronounced dislocation substructure. One could speculate that the observed irregular appearance of QF boundaries might be a consequence of a morphological instability of the advancing austenite/ferrite interfaces.[41] However, a recent detailed metallographic study of the early stages of ferrite formation at the prior-austenite grain boundaries below the Widmanstätten start temperature[42] showed only rare indications of the aforementioned instability. Instead, the ragged character of the ferrite grains observed in Reference 42 was largely a consequence of their development involving the nucleation and growth of both primary and secondary WF sideplates, termed according to the Dube classification system.[43] As a result of mutual impingement of the growing WF sideplates, these grains (including the apparent grain-boundary allotriomorphs) were mostly composed of fragments, containing high dislocation densities and separated by low-angle boundaries, and often contained small embedded islands of the austenite stabilized against further transformation to ferrite.[42] Thus, the aforementioned ferrite grain characteristics resembled closely those of the QF grains observed in the present study. This appears to support the view presented by Bee and Honeycombe[44] that QF (or "massive ferrite") might essentially result from the WF transformation reaching its completion.

However, only ferrite morphological forms which evolved directly from the (apparent) grain-boundary allotriomorphs[42] were classified as QF grains in the present study, according to the adopted nomenclature,[7] while the rest of the microstructure was tentatively classified as GF. This implies that, in the context of the present investigation, the microstructure observed in Reference 44 might actually represent a mixture of QF and GF. Indeed, on the basis of careful comparisons of the ferrite microstructures classified as QF or GF in the present work[7] with those available in the literature, it appears that the aforementioned constituents are essentially products of WF transformation.[25,26,42,44,45] The observation that QF requires relatively higher temperatures for its formation, whereas GF is characterized by comparatively lower transformation temperatures, might be explained using a concept presented by Okaguchi *et al.*[45] According to this concept, ferrite nuclei formed at the austenite grain boundary, which are generally (semi-)coherent with at least one of the austenite grains separated by this boundary,[37,38] may grow into both the grains at the relatively high QF formation temperatures. This is consistent with the elimination of the locations of the prior-austenite grain boundaries during the QF growth observed in the present study. The observed ragged character of QF grains appeared to be largely caused by the formation of small secondary WF sideplates, nucleated sympathetically on the pre-existing (apparent) grain-boundary allotriomorphs[42] and further modified in shape during their growth by diffusional processes.[45]

According to Okaguchi *et al.*,[45] a decrease in transformation temperatures to the level observed in steels D and H will reduce the diffusion distance, and, as a result, the growth of the grain-boundary ferrite nuclei will largely proceed by the movement of their (semi-)coherent interfaces with the austenite. Consequently, it can be expected that the formation of QF might become effectively suppressed and the locations of the prior-austenite grain boundaries might remain preserved, which was indeed observed in the aforementioned steels, the microstructure of which was dominated by GF. Thus, in this case, GF appears to have largely developed from primary WF sideplates[43] nucleating directly on the prior-austenite grain boundaries, possibly complemented by WF plates nucleating intragranularly. Conversely, when GF was formed together with QF, it appears to have predominantly developed from secondary WF sideplates[43] nucleated on the pre-existing grain-boundary ferrite allotriomorphs (which further evolved into QF grains), as well as from intragranular WF plates. After the complete transformation, the GF crystals were observed to have shapes close to irregular coarse rods, displaying both elongated and roughly equiaxed complex cross sections, which indicates that the shape of the original WF plate-like (lath-like) nuclei was substantially modified during their growth. It has been proposed that the WF plates could gradually acquire more irregular "degenerate" shapes *via* localized diffusional sidewise growth and lath coalescence[45] or sympathetic nucleation of additional ferrite crystals.[25,26]

It seems reasonable to suggest that the increased dislocation densities found within both QF grains and GF crystals originated mainly from accommodation of the stresses, caused by a volume change accompanying the transformation at the relatively low temperatures involved. The frequently observed low-angle boundaries, subdividing the aforementioned grains or sheaves into smaller fragments, appear to have largely resulted from mutual impingement of several growing ferrite crystals, formed by separate nucleation events or sympathetically.[42] Consequently, it could be expected that some carbon-enriched austenite regions, stabilized against further transformation to ferrite, might become entrapped locally between the growing QF or GF crystals. Indeed, such local volumes, transformed during subsequent cooling to either bainite or M/A microconstituents, were frequently observed in the present study, especially within GF sheaves.

The microstructural characteristics of the remaining non-equilibrium ferrite constituent, BF, were found to display certain similarities to those of GF. The locations of the prior-austenite grain boundaries remained preserved after the complete transformation. The low-angle boundaries between individual ferrite crystals, comprising the BF packets, clearly resulted from mutual impingement of growing nuclei, formed either individually or sympathetically. The high dislocation densities observed within these crystals probably originated largely from accommodation of the stresses caused by the volume change, or perhaps also from the lattice invariant strain.[30] However, unlike the GF crystals having shapes of irregular coarse rods, their BF counterparts

appeared to be predominantly platelike, systematically displaying lathlike cross sections. Consequently, the carbon-enriched M/A microregions, situated along the boundaries separating individual BF plates, displayed an acicular morphology, whereas those embedded within GF sheaves were largely roughly equiaxed.

It has been suggested[46] that the formation mechanism of BF might be essentially the same as that of GF, the only difference being a significantly lower level of degeneration accompanying the growth of the latter microstructural constituent, due to the extremely short transformation time intervals available for the BF formation. However, the transformation temperatures corresponding to BF were generally found to be noticeably lower than their GF counterparts, as illustrated by the CCT diagrams of steels D and H (Figures 2(g) and (h) and 3(g) and (h)), which indicates that the respective transformation mechanisms might not be the same. The BF might perhaps represent a genuine "bainitic" microstructure, alternatively classified by Ohmori *et al.*[11] as BI carbide-free upper bainite, in correspondence with the nomenclature adopted in the present work.[7] It is beyond the scope of the present work to attempt to comment on the nature of the formation mechanisms of the nonequilibrium ferrite constituents that are still under dispute.[28–30,45,47,48] Nevertheless, the presence of carbon-enriched bainite or M/A microregions, observed within the aforementioned constituents even in the ultralow-carbon steels A through D, which have carbon contents well below the solubility limit in ferrite, indicates that the corresponding austenite/ferrite interface regions may be significantly enriched in carbon.[48,49]

There appeared to be no significant change in morphology of the transformation products derived from the heavily deformed, unrecrystallized austenite, when compared to the microstructures formed from the recrystallized austenitic matrix, apart from the observed refinement of the PF and QF grains, as well as the GF and BF assemblies. This microstructural refinement may be largely attributed to a significant increase in the density of potential ferrite nucleation sites introduced by deformation,[31–35] as discussed previously. The slightly enhanced fragmentation of GF sheaves, observed in samples derived from the deformed austenite, might possibly be attributed to nucleation of the ferrite crystals in neighboring, slightly misoriented regions present within the deformed parent austenite grains.[34]

The terminology proposed by the Bainite Research Committee of the Iron and Steel Institute of Japan[7] was adopted in the present work for the reason that this terminology has been widely used in the technological literature in both its original[7] and modified[8] forms. This will, thus, facilitate a direct comparison of the present results with a majority of those available in the literature. Also, it is important that the aforementioned nomenclature be able to distinguish between the nonequilibrium ferrite constituents, termed QF and GF on the basis of their morphological features, as their opposite tendency toward conserving the prior-austenite grain boundaries will have an impact on the resulting mechanical properties. The results of the present investigation indicate that the aforementioned constituents might possibly represent WF transformation products undergoing significant degeneration during their growth, and, thus, they might be perhaps alternatively referred to as two forms of "degenerate" WF. However, more fundamental research work is needed to clarify the transformation mechanisms for the nonequilibrium ferrite constituents in general. Such clarification would, perhaps, make it possible to propose an improved nomenclature for the aforementioned constituents, descriptive of not only morphological features but also the formation mechanisms.

C. *Hardness Characteristics*

The systematically higher hardness values displayed by the low-carbon steels E through H, compared to those observed in their ultralow-carbon counterparts A through D for similar microstructures, are believed to be primarily a consequence of the significantly finer transformation microstructures generally found in the former group of steels, the respective carbon levels being of secondary importance. Microstructural refinement might be similarly suggested to account for the observed increased hardness values of the transformation products formed from the deformed austenite, in comparison with those of the equivalent microstructures created from the recrystallized austenitic matrix. The observed inversely proportional relationship linking hardness and the transformation start temperatures, which appeared to be rather insensitive to the particular steel composition, suggests that the microalloying additions of boron and molybdenum increase hardness predominantly through enhancing hardenability and modifying the resultant transformation microstructures. Any contribution from solid-solution strengthening by molybdenum appears to be less significant. The pronounced hardness plateaus extending over a wide range of cooling rates, displayed by the transformation microstructures dominated by GBF in steels C, D, and H, can be expected to ensure uniform mechanical properties across large cross sections, generally characterized by significant differences in cooling rates between local volumes. This might be beneficial for the thermomechanical processing of the aforementioned steels.[4]

V. CONCLUSIONS

The effects of composition and prior-austenite deformation on the transformation characteristics of a group of low-carbon and ultralow-carbon microalloyed steels, containing hardenability-enhancing additions of boron and/or molybdenum, have been studied using deformation dilatometry. From this investigation, the following main conclusions can be drawn.

1. Individual additions of molybdenum (0.3 wt pct) appeared to slightly increase the hardenability of the base steel at the low carbon (0.04 wt pct) level, while there was barely a detectable change in hardenability observed at the ultralow carbon (0.007 wt pct) concentration.
2. Individual additions of boron (0.002 wt pct) to the base steel composition were found to be significantly more effective in promoting hardenability than those of molybdenum, markedly restricting the formation of polygonal ferrite at the low carbon content and completely eliminating this constituent at the ultralow carbon concentration over the entire range of cooling rates studied (0.1 °C/s to 100 °C/s).
3. A comparatively large increase in hardenability was achieved by combined additions of molybdenum and

boron to the base steel composition, and the resultant transformation behavior appeared similar for the two carbon levels studied. The transformation temperatures were lowered significantly, the formation of polygonal ferrite was entirely eliminated, and that of quasi-polygonal ferrite was markedly suppressed.

4. In those steels in which polygonal ferrite was formed, heavy austenite deformation (>0.45 strain in compression) brought about a significant decrease in hardenability due to enhanced formation of this microstructural constituent.
5. Those steels in which exclusively nonequilibrium ferrite microstructures were formed mostly displayed a fairly small decrease in hardenability, suggesting that the transformation mechanisms for these constituents are significantly less sensitive to deformation than that for polygonal ferrite.
6. Carbon-enriched islands, present within the polygonal ferrite matrix at the low carbon content, were found to be composed predominantly of classical bainite, accompanied by small fractions of fine pearlite or degenerate pearlite.
7. Both quasi-polygonal and granular ferrite might possibly represent Widmanstätten ferrite transformation products undergoing significant degeneration during its growth, whereas bainitic ferrite appears to represent a "genuine" bainitic microstructure having a different formation mechanism.
8. Carbon-enriched microregions, present within the nonequilibrium ferrite microstructures at both carbon levels studied, consisted primarily of martensite/austenite microconstituents, largely composed of lath martensite with only a barely detectable fraction of retained austenite. The presence of these microregions in the ultralow-carbon steels implies significant local enrichment in carbon within the vicinity of the austenite/ferrite interface.
9. Those ferrite microstructures obtained after transformation from heavily deformed, unrecrystallized austenite were generally found to be of a significantly finer scale and more fragmented than those formed from recrystallized austenite.
10. The additions of molybdenum and/or boron appeared to increase hardness primarily through enhancing hardenability and modifying the resultant transformation microstructures. Any contribution from solid-solution strengthening by molybdenum appeared to be less significant.

ACKNOWLEDGMENTS

The authors acknowledge gratefully the support of an Australian Research Council Collaborative Research Grant in conjunction with BHP Research–Melbourne Laboratories.

REFERENCES

1. G.I. Garcia: *Proc. Int. Conf. Microalloying '95*, The Iron and Steel Society, Warrendale, PA, 1995, pp. 365-75.
2. B.A. Graville: *Proc. Int. Conf. Welding of HSLA Structure Steels*, ASM, Metals Park, OH, 1978, pp. 85-101.
3. T. Araki: *Proc. Int. Conf. HSLA Steels '85*, J.M. Gray *et al.*, eds., ASM INTERNATIONAL, Metals Park, OH, 1986, pp. 259-71.
4. I. Tamura, H. Sekine, T. Tanaka, and C. Ouchi: *Thermomechanical Processing of High-Strength Low-Alloy Steels*, Butterworth and Company, London, 1988, pp. 1-248.
5. Y.E. Smith, A.P. Coldren, and R.L. Cryderman: *Toward Improved Ductility and Toughness*, Iron and Steel Institute of Japan, Tokyo, 1971, pp. 119-42.
6. B.P. Wynne, P. Cizek, C.H.J. Davies, B.C. Muddle, and P.D. Hodgson: *Proc. Int. Conf. THERMEC '97*, T. Chandra and T. Sakai, eds., TMS, Warrendale, PA, 1997, vol. 1, pp. 837-43.
7. *Atlas for Bainitic Microstructures—Vol. 1, Continuous-Cooled Zw Microstructures of Low-Carbon Steels*, T. Araki *et al.*, eds., Iron and Steel Institute of Japan, Tokyo, 1992, pp. 4-5.
8. B.L. Bramfitt and J.G. Speer: *Metall. Trans. A*, 1990, vol. 21A, pp. 817-29.
9. G. Krauss and S.W. Thompson: *Iron Steel Inst. Jpn. Int.*, 1995, vol. 35, pp. 937-45.
10. H.K.D.H. Bhadeshia: *Bainite in Steels*, Transformations, Microstructure and Properties, The Institute of Materials, London, 1992, pp. 245-82.
11. Y. Ohmori, H. Ohtani, and T. Kunitake: *Trans. Iron Steel Inst. Jpn.*, 1971, vol. 11, pp. 250-59.
12. J.R. Yang, C.Y. Huang, and S.C. Wang: *Proc. Int. Symp. Low-Carbon Steels for the 90's*, R. Asfahani and G. Tither, eds., TMS, Warrendale, PA, 1993, pp. 293-301.
13. J.R. Yang, C.Y. Huang, and C.S. Chiou: *Iron Steel Inst. Jpn. Int.*, 1995, vol. 35, pp. 1013-19.
14. S. Yamamoto, H. Yokoyama, K. Yamada, and M. Niikura: *Iron Steel Inst. Jpn. Int.*, 1995, vol. 35, pp. 1020-26.
15. P.A. Manohar, T. Chandra, and C.R. Killmore: *Iron Steel Inst. Jpn. Int.*, 1996, vol. 36, pp. 1486-93.
16. H. Tamehiro, M. Murata, and R. Habu: *Proc. Int. Conf. HSLA Steels '85*, J.M. Gray *et al.*, eds., ASM INTERNATIONAL, 1986, pp. 325-33.
17. G. Spanos, H.S. Fang, and H.I. Aaronson: *Metall. Trans. A*, 1990, vol. 21A, pp. 1381-90.
18. Ph. Maitrepierre, J. Rofes-Vernis, and D. Thivellier: *Proc. Int. Symp. Boron in Steels*, S.K. Banerji and J.E. Morral, eds., TMS-AIME, Warrendale, PA, 1980, pp. 1-18.
19. J.S. Kirkaldy, B.A. Thomson, and E.A. Baganis: in *Hardenability Concepts with Applications to Steel*, D.V. Doane and J.S. Kirkaldy, eds., TMS-AIME, Warrendale, PA, 1978, pp. 82-125.
20. J.E. Morral and T.B. Cameron: *Proc. Int. Symp. Boron in Steels*, S.K. Banerji and J.E. Morral, eds., TMS-AIME, Warrendale, PA, 1980, pp. 19-32.
21. M. Enomoto, C.L. White, and H.I. Aaronson: *Metall. Trans. A*, 1988, vol. 19A, pp. 1807-18.
22. R.C. Sharma and G.R. Purdy: *Metall. Trans.*, 1974, vol. 5, pp. 939-47.
23. M. Enomoto, N. Nojiri, and Y. Sato: *Mater. Trans. JIM*, 1994, vol. 35, pp. 859-67.
24. M. Enomoto and H.I. Aaronson: *Metall. Trans. A*, 1986, vol. 17A, pp. 1385-97.
25. W.T. Reynolds, Jr., F.Z. Li, C.K. Shui, and H.I. Aaronson: *Metall. Trans. A*, 1990, vol. 21A, pp. 1433-63.
26. J.K. Chen, R.A. Vandermeer, and W.T. Reynolds, Jr.: *Metall. Mater. Trans. A*, 1994, vol. 25A, pp. 1267-79.
27. H.I. Aaronson: *Metall. Trans. A*, 1993, vol. 24A, pp. 241-76.
28. W.T. Reynolds, Jr., H.I. Aaronson, and G. Spanos: *Mater. Trans. JIM*, 1991, vol. 32, pp. 737-46.
29. Y. Ohmori and T. Maki: *Mater. Trans. JIM*, 1991, vol. 32, pp. 631-41.
30. H.K.D.H. Bhadeshia and J.W. Christian: *Metall. Trans. A*, 1990, vol. 21A, pp. 767-97.
31. G.R. Speich, L.J. Cuddy, C.R. Gordon, and A.J. DeArdo: in *Phase Transformations in Ferrous Alloys*, A.R. Marder and J.I. Goldstein, eds., TMS-AIME, Warrendale, PA, 1983, pp. 341-89.
32. E. Essadiqi and J.J. Jonas: *Metall. Trans. A*, 1988, vol. 19A, pp. 417-26.
33. I. Tamura, H. Sekine, T. Tanaka, and C. Ouchi: *Thermomechanical Processing of High-Strength Low-Alloy Steels*, Butterworth and Co., London, 1988, pp. 86-93.
34. P. Cizek, B.P. Wynne, B.C. Muddle, and P.D. Hodgson: *Proc. Int. of Conf. THERMEC '97*, T. Chandra and T. Sakai, eds., TMS, Warrendale, PA, 1997, vol. 1, pp. 709-15.
35. H. Inagaki: *Trans. Iron Steel Inst. Jpn.*, 1983 vol. 23, pp. 1059-67.
36. P.H. Shipway and H.K.D.H. Bhadeshia: *Mater. Sci. Technol.*, 1995, vol. 11, pp. 1116-28.
37. E.A. Wilson: *Met. Sci.*, 1984, vol. 18, pp. 471-84.
38. E.A. Wilson: *Iron Steel Inst. Jpn. Int.*, 1994, vol. 34, pp. 615-30.

39. B. Bay, N. Hansen, D.A. Hughes, and D. Kuhlmann-Wilsdorf: *Acta Metall. Mater.*, 1992, vol. 40, pp. 205-19.
40. S.W. Thompson, D.J. Colvin, and G. Krauss: *Metall. Mater. Trans. A*, 1996, vol. 27A, pp. 1557-71.
41. R.D. Townsend and J.S. Kirkaldy: *Trans. ASM*, 1968, vol. 61, pp. 605-19.
42. G. Spanos and M.G. Hall: *Metall. Mater. Trans. A*, 1996, vol. 27A, pp. 1519-34.
43. C.A. Dube, H.I. Aaronson, and R.F. Mehl: *Rev. Met.*, 1958, vol. 55, p. 201.
44. J.V. Bee and R.W.K. Honeycombe: *Metall. Trans. A*, 1978, vol. 9A, pp. 587-93.
45. S. Okaguchi, H. Ohtani, and Y. Ohmori: *Mater. Trans. JIM*, 1991, vol. 32, pp. 697-704.
46. G. Spanos, R.W. Fonda, R.A. Vandermeer, and A. Matuszeski: *Metall. Mater. Trans. A*, 1995, vol. 26A, pp. 3277-93.
47. F. Hongsheng, Z. Yankang, and B. Bingzhe: *Proc. Int. Conf. HSLA Steels '85*, J.M. Gray *et al.*, eds., ASM INTERNATIONAL, Metals Park, OH, 1986, pp. 359-67.
48. T. Araki, K. Shibata, and H. Nakajima: *Proc. Int. Conf. ICOMAT '92*, C.M. Wayman and J. Perkins, eds., Monterey Institute for Advanced Studies, Monterey, CA, 1993, pp. 767-72.
49. K. Shibata and K. Asakura: *Iron Steel Inst. Jpn. Int.*, 1995, vol. 35, pp. 982-91.